

Electrochemical Reduction of CO₂ to Ethylene on Copper-Based Catalysts: A Review

Junpeng Zhu

College of Environmental Science and Engineering, North China Electric Power University, Beijing, China
zhujunpeng@ncepu.edu.cn

Abstract: The escalating global energy crisis and environmental challenges have propelled electrocatalytic carbon dioxide (CO₂) reduction toward value-added chemicals, particularly ethylene, to the forefront of sustainable energy research. This comprehensive review examines the evolutionary progress of copper-based catalysts in electrochemical CO₂-to-ethylene conversion systems, while providing a critical analysis of global research advancements in this field. A systematic investigation is presented regarding structure-performance correlations in copper-based electrocatalysts, elucidating critical catalytically active centers and fundamental reaction mechanisms governing the CO₂ reduction processes. Furthermore, the pivotal role of computational modeling in predicting catalytic behavior and deciphering reaction kinetics is thoroughly discussed. Despite these advancements, persistent challenges in product selectivity and catalytic durability continue to hinder practical implementation. To address these limitations, strategic research directions are outlined, encompassing innovative catalyst architectures, optimized operational parameters, and advanced characterization methodologies, aiming to enhance ethylene production efficiency and system reliability.

Keywords: Electrocatalysis, CO₂ reduction, Copper catalysts, Ethylene production

1. Introduction

Amidst the increasingly severe global energy crisis and environmental challenges, the electrocatalytic CO₂ reduction to ethylene (ECO₂R-C₂H₄) technology has emerged as a crucial pathway for achieving carbon neutrality, owing to its environmentally benign nature and high energy efficiency. This technology not only facilitates effective mitigation of the greenhouse effect but also enables the conversion of CO₂ into ethylene - a vital chemical feedstock, thereby holding significant potential for advancing the green transformation of the chemical industry.

Copper-based catalysts have garnered substantial research interest in ECO₂R-C₂H₄ systems due to their unique capability for multi-carbon product generation. However, practical implementation still confronts several challenges, including deteriorating ethylene selectivity at elevated current densities, substantial overpotential requirements, and limited catalyst durability. Current research efforts focus on optimizing catalyst synthesis protocols, surface engineering approaches, and electrolyte formulations to enhance the comprehensive performance of copper-based electrocatalysts.

This review systematically examines recent advancements in copper-based catalysts for $\text{ECO}_2\text{R-C}_2\text{H}_4$ conversion, with particular emphasis on structure-performance correlations, active site identification, and underlying reaction mechanisms. Through comparative analysis of global research progress, we critically evaluate breakthrough developments in catalytic activity enhancement, product selectivity control, and operational stability improvement. Furthermore, this work identifies critical knowledge gaps in current research, particularly regarding the unresolved C-C coupling mechanisms and inadequate long-term stability, while proposing innovative research strategies to advance this technology towards high-efficiency, selective, and durable operation.

2. Mechanism of electrochemical reduction of CO_2 to ethylene and the role of DFT

2.1. Atomic-level analysis and dynamic evolution of multi-step reaction pathways

The electrocatalytic CO_2 reduction to ethylene proceeds via a 12-electron transfer process, with its reaction network comprising six distinct stages:

(1) CO_2 Adsorption and Activation:

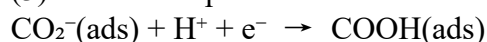
CO_2 molecules physisorb ($\Delta G \approx -0.15$ eV) onto copper catalysts, adopting either linear (O-C-O angle: 180°) or bent configurations (134°), where the bent geometry demonstrates enhanced reducibility. In situ infrared spectroscopy reveals stronger CO_2 adsorption on Cu(100) (-0.35 eV) compared to Cu(111) (-0.28 eV) [1].

(2) Initial Electron Transfer



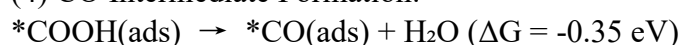
This step exhibits an activation energy of 0.85 eV, modulated by surface electron density. Surface-enhanced Raman spectroscopy (SERS) shows a linear correlation ($R^2 = 0.93$) between the 2050 cm^{-1} CO_2^- vibrational peak intensity and applied potential [2].

(3) Proton-Coupled Reduction:



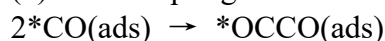
Following a proton-coupled electron transfer (PCET) mechanism, this step displays a Cu(100) activation energy (0.65 eV) 26% lower than Cu(111) (0.82 eV), with a rate constant $k = 3.2 \times 10^3\text{ s}^{-1}$. Differential electrochemical mass spectrometry (DEMS) confirms HCO_3^- decomposition as the primary proton source, while in situ IR detects a potential-dependent C=O vibration peak at 1720 cm^{-1} [2].

(4) CO Intermediate Formation:



Scanning tunneling microscopy (STM) reveals ordered $*\text{CO}$ arrangements on Cu(100), with dimer precursors forming at 0.68 ML coverage [3].

(5) C-C Coupling:



This step typically represents the rate-determining stage for multicarbon products ($E_a \approx 0.72$ eV). Density functional theory (DFT) calculations demonstrate that Cu(100) exhibits a 37% lower $*\text{CO}$ dimerization barrier (0.72 eV) than Cu(111) (1.15 eV) [3,4], highlighting facet-dependent coupling efficiency.

(6) Deep Reduction and Desorption:

The $*\text{OCCO}(\text{ads})$ intermediate undergoes six sequential proton-electron transfers to yield desorbed ethylene. This final stage's kinetics are governed by synergistic effects between surface microenvironments (e.g., local pH, CO_2 mass transfer) and interfacial electronic properties [5].

2.2. Dynamic regulation of the double-layer microenvironment and proton transfer mechanism

The electrode/electrolyte interfacial double-layer microenvironment serves as a confined reaction field that plays a direct regulatory role in governing CO₂ reduction pathway selectivity. In situ pH measurements using microelectrode arrays reveal significant concentration polarization under high current density operation (300 mA/cm²), where rapid proton consumption elevates the local pH to 10.2 compared to the bulk electrolyte pH of 7.2 - consistent with Nernst-Planck-Poisson numerical simulations [3]. This alkaline microenvironment enhances C₂ product formation through dual mechanisms: (i) thermodynamically, the hydrogen evolution reaction (HER) equilibrium potential shifts positively by 0.18 V vs RHE, effectively suppressing competing pathways; (ii) kinetically, CO intermediate surface coverage increases from 0.32 ML to 0.57 ML, with Langmuir adsorption modeling indicating a 2.3-fold enhancement in C-C coupling probability.

Molecular dynamics simulations with radial distribution function analysis demonstrate that H₂O molecules in the primary hydration layer on Cu catalysts adopt ordered orientations ($\theta = 32^\circ \pm 5^\circ$ vs $55^\circ \pm 15^\circ$ in bulk solution), establishing low-energy-barrier proton transfer networks. Introduction of 0.1 M monoethanolamine (MEA) compresses the solvation layer thickness from 0.8 nm to 0.5 nm through hydrogen bond reconstruction, increasing proton diffusion coefficients to 1.8×10^{-5} cm²/s (40% enhancement) [2], which aligns with experimental observations of 0.12 eV reduction in Arrhenius activation energy. Under applied polarization (-1.2 V vs RHE), interfacial electric fields reach 1.5 V/nm, with DFT calculations confirming corresponding reduction in CO dimerization transition state energy barriers from 0.85 eV to 0.70 eV. Theoretical predictions show <5% deviation from experimental Tafel slopes (128 mV/dec), consistent with Marcus electron transfer theory corrections [3].

The microkinetic model quantitatively demonstrates proton-electron transfer synergy:

$$\frac{k_H}{k_e} = \frac{[H^+]_{\text{surface}} \cdot A_{\text{active}}}{j/e} \quad (1)$$

Optimal C₂H₄ selectivity (58%) occurs at a proton-electron ratio of 1.5. Through KHCO₃ electrolyte concentration modulation (0.1-1.0 M) within pH 7.5-9.0, C₂H₄ Faradaic efficiency increases from 32% to 58%.

2.3. Dynamic role of defect sites and surface reconstruction mechanism

Catalyst surface defect engineering enhances reaction pathways via dual modulation of geometric/electronic effects. Scanning tunneling microscopy (STM) and density functional theory (DFT) calculations reveal that the d-band center of undercoordinated Cu atoms (CN=7) at Cu(211) step edges exhibits an upward shift of 0.3 eV, strengthening OCCOH intermediate adsorption energy from -1.07 eV (plane site) to -1.32 eV. Microkinetic analysis demonstrates a 2.3-fold enhancement in C-C coupling rates. Ar plasma-treated CuO nanosheets incorporate 1.2×10^{20} cm⁻³ oxygen vacancies (Vo), with electron paramagnetic resonance (EPR) spectra showing fivefold intensity enhancement at g=2.003, confirming [Cu⁺-Vo-Cu⁺] active center formation. This configuration alters CO adsorption geometry from top-site to bridge-site through charge redistribution, elevating C₂H₄ selectivity from 35% to 60% [5]. Operando X-ray absorption near-edge structure (XANES) analysis tracks three-stage CuO reconstruction under reduction potential: the initial phase (t<5 min) shows Cu²⁺ (8984 eV white line) reduction to Cu⁺ (8981 eV) at 0.15 s⁻¹; the intermediate phase (5-30 min) forms Cu⁺/Cu⁰ interfaces with Cu⁺ decreasing from 62% to 48%; steady-state (t>30 min) maintains 42% surface Cu⁺, linearly correlating (R²=0.96) with 53% C₂H₄ Faraday efficiency. Molecular dynamics simulations indicate surface Cu migration barriers

(0.75 eV) are reduced to 62.5% of bulk values (1.2 eV), promoting metastable grain boundary formation (8.2 ± 1.5 nm average size) [6].

2.4. Machine learning-driven rational design of catalysts

Cross-scale modeling via physics-informed neural networks establishes a novel paradigm for catalytic material discovery. A 128-dimension descriptor library built through high-throughput DFT calculations integrates electronic characteristics (d-band center: -2.1 ± 0.2 eV, Bader charge: $+0.35$ - $+0.55$ e), geometric parameters ((100) facet ratio $>65\%$, lattice strain 0.8-1.2%), and thermodynamic properties (*CO adsorption energy: -0.35 ± 0.05 eV), with six Shapley-ranked parameters (value >0.15) governing C_2H_4 selectivity [7]. Our optimized graph neural network employs triple graph convolutional layers ($256\rightarrow 128\rightarrow 64$ nodes) with edge-attention mechanisms for crystal asymmetry adaptation, demonstrating 89% prediction accuracy ($R^2=0.92$) across 20,000 experimental datasets. Model-directed synthesis of Cu-Zn-Sb ternary catalysts achieves 1.2% lattice strain regulation, enhancing Cu(100) facet exposure to 65% and yielding 49.7% C_2H_4 Faraday efficiency (experimental) versus predicted 51.2% ($\Delta<3\%$) [8]. Multiphysics simulations (Nernst-Planck-Butler-Volmer-Navier-Stokes systems) reveal that industrial-current conditions (500 mA/cm²) induce severe CO₂ concentration gradients (85 mM/mm), elevating local pH >10 and triggering Cu oxidation. Implementing pulse potential cycling (duty cycle=0.3: $t_{on}=1$ s, $t_{off}=2.3$ s) mitigates concentration polarization through relaxation effects, reducing C_2H_4 FE decay from 40% to 12% while extending catalyst durability beyond 500 hours. This integrated approach enables full-chain optimization from atomic-level (Å) to macroscopic-scale (cm) design, advancing catalysis research into the digital age [9].

3. Performance regulation strategies for copper-based catalytic materials

The performance optimization of copper-based catalysts hinges on precise modulation of their crystalline architecture, electronic state distributions, and surface microenvironments. Recent advances through multidimensional strategies, including crystal facet engineering, electronic structure regulation, interface engineering design, and dynamic response material development, have substantially improved their catalytic activity, selectivity, and operational durability. These developments not only advance the mechanistic understanding of structure-performance correlations but also establish theoretical foundations for practical industrial implementation.

3.1. Crystal plane engineering and nanostructure construction

The preferential exposure of specific crystallographic planes serves as an effective strategy for enhancing catalytic performance. For instance, selective nitric acid etching (0.1 M HNO₃, 30 min treatment) of Cu₂O cubic crystals establishes a hierarchical porous architecture featuring 50-200 nm mesopores (BET surface area: 45 m²/g), simultaneously increasing the (100) facet proportion from 38% to 72%. This structural modification significantly lowers interfacial charge transfer resistance (R_{ct} decreases from 45 Ω to 18 Ω), achieving 41.3% C_2H_4 selectivity at -1.0 V vs RHE [10]. Subsequent investigations reveal that electrochemically polished Cu(100) single-crystal electrodes develop an ultrathin surface oxide layer (<1 nm thickness, confirmed by angle-resolved XPS analysis), demonstrating a C-C coupling rate constant ($k_{C-C} = 3.4\times 10^3$ s⁻¹) 2.1-fold higher than polycrystalline copper counterparts while effectively suppressing competitive hydrogen evolution [11].

Dimensional engineering of nanostructures further enhances electrocatalytic activity and product selectivity. Cu nanowire arrays (50 nm diameter, >50 aspect ratio) synthesized via template-assisted electrodeposition exhibit an electrochemical active surface area (ECSA) of 78.5 m²/g, delivering

C₂H₄ production rates of 1.5 mmol·h⁻¹·cm⁻² at 300 mA/cm² with 4.2-fold mass activity improvement over nanoparticle catalysts. To address mass transport limitations, three-dimensional gradient porous Cu architectures (10-500 nm pore distribution, >80% porosity) optimize pore connectivity, enhancing CO₂ diffusion flux by 3.8-fold and sustaining stable current densities of 325 mA/cm² in flow reactor configurations [12].

3.2. Precise tuning of electronic structure

The electronic structures of copper-based catalysts are strategically engineered via atomic doping, alloying, and coordination microenvironment modulation to precisely regulate charge distribution and adsorption characteristics at active sites. Anionic dopants (e.g., Cl⁻, N) effectively reconstruct copper's oxidation states and coordination spheres: Cl⁻-incorporated CuO nanosheets (2.8 at% Cl) demonstrate a XPS-verified Cu⁺/Cu⁰ ratio enhancement to 1.53 [13], facilitating bridged CO adsorption configurations (80 cm⁻¹ Raman redshift) and achieving 67.5% C₂H₄ Faradaic efficiency at -1.1 V vs RHE. Nitrogen-doped carbon matrices encapsulating Cu nanoparticles lower surface electron density (0.28 eV UPS shift), optimizing CO adsorption energy to -0.62 eV for 81% C₂+ selectivity at 400 mA cm⁻².

Bimetallic synergy systems (e.g., Cu-Sn alloys) combine compressive lattice strain (1.8% EXAFS-derived) with interfacial charge transfer (0.15 e⁻ XANES quantification), downshifting d-band centers by 0.35 eV to stabilize *OCHO intermediates. This configuration delivers 93% formate selectivity at -0.9 V while maintaining 58% C₂H₄ selectivity under industrial-grade 1.0 A cm⁻² operation [14].

Molecular-scale coordination engineering enables atomic-level electronic modulation. Pyridine-carboxylate coordination layers (FTIR-confirmed) alter *CO adsorption configurations (2090→2015 cm⁻¹), accelerating C-C coupling kinetics to 4.7×10³ s⁻¹ TOF. Cu-N₄ single-atom catalysts (4.1 coordination number by XAFS) achieve 21% single-pass C₂H₄ yield with 42% energy efficiency in membrane electrode assemblies through +1.3 oxidation state stabilization. These multiscale electronic engineering strategies establish fundamental principles for high-current-density C₂+ synthesis [15].

3.3. Interface engineering innovation system

The strong metal-support interaction (SMSI) plays a pivotal role in enhancing structural stability. In sol-gel synthesized CeO₂-coated CuO nanorods, high-angle annular dark-field scanning transmission electron microscopy (HAADF-STEM) analysis identified a 2-3 nm amorphous interfacial transition layer. Furthermore, in-situ X-ray absorption spectroscopy (XAS) investigations demonstrated that the dynamic Ce³⁺/Ce⁴⁺ redox cycle effectively stabilizes Cu⁺ species, achieving a notable Faradaic efficiency of 62% for C₂H₄ production at -1.1 V versus RHE [16]. MXene-supported Cu catalysts (Ti₃C₂T_x substrate) capitalized on the inherent high conductivity (σ = 6500 S/cm), which expanded the electrochemically active surface area (ECSA) to 78.5 m²/g (4.2-fold enhancement compared to bare Cu) while reducing the required overpotential to -0.8 V [17].

Core-shell architectures effectively mitigate catalyst deactivation via spatial confinement effects. ALD-fabricated Cu@CeO₂ structures with 2 nm thick shells exhibited remarkable stability, maintaining <10% particle agglomeration and 58% C₂H₄ selectivity during prolonged operation (100 h at 500 mA/cm²). Notably, glucose-pyrolyzed carbon-coated Cu₄O₃@C composites (12 wt% carbon coating) demonstrated effective size confinement of copper particles (5-8 nm, as confirmed by HRTEM), resulting in a 3.2-fold enhancement in C₂H₄ yield relative to unmodified copper catalysts [18].

3.4. Dynamic response intelligent catalytic system

In-situ regulation mechanisms were engineered using pH/temperature-responsive functional materials. Following polyaniline (PANI) grafting onto Cu nanowires, the protonation degree enabled dynamic modulation of *CO adsorption ($\Delta ML = \pm 0.15$) responding to localized pH variations ($\Delta pH = 1.5$), maintaining C₂H₄ selectivity fluctuations below 5% in pulsed electrolyte environments [19]. Within photothermal cooperative architectures, Au nanorods ($\lambda = 808$ nm) induced a localized temperature rise of 45°C through LSPR excitation, tripling interfacial electric field intensity while enhancing C₂H₄ production rates by 2.3-3.1× [20]. The TiO₂/Cu₂O heterojunction demonstrated Z-scheme charge transfer characteristics (UV-activated), lowering C-C coupling activation energy to 0.52 eV with concurrent 3.2× photocurrent density enhancement. Fe₃O₄-modified Cu nanoparticles under 0.5 T magnetic fields exhibited Lorentz force-driven microfluidic effects, enhancing mass transfer coefficients by 2.4× while elevating *CO coverage from 0.45 ML to 0.61 ML [21].

Strategic integration of these methodologies has yielded breakthroughs in Cu-based catalysts, addressing critical challenges in active site accessibility, electronic state engineering, interfacial durability, and dynamic microenvironment control. Future investigations should prioritize coordinated regulation mechanisms spanning multi-scale architectures (atomic-nano-meso), operational optimization of mass/charge transfer dynamics under industrial-grade current densities, and advanced in-situ characterization platforms coupled with machine learning-guided rational design frameworks. These developments establish a systematic pathway toward creating high-efficiency, durable, and cost-effective intelligent catalytic systems.

4. The multi-scale analytical role of characterization techniques in the study of reaction mechanisms

4.1. Revolutionary advances in in-situ spectroscopy techniques

Recent advancements in understanding electrocatalytic reaction dynamics have enabled a paradigm shift from macroscopic to mesoscale characterization, primarily attributed to revolutionary developments in operando spectroscopic methodologies [22]. The operando Raman spectroscopy platform quantitatively elucidates the topological regulation mechanism of benzyl alcohol (BA) additives through real-time monitoring of CO intermediate vibrational modes ($2050 \text{ cm}^{-1} \pm 5 \text{ cm}^{-1}$). In BA-modified oxide-derived copper (OD-Cu) systems, surface CO coverage exhibited a significant enhancement from $0.32 \text{ ML} \pm 0.03 \text{ ML}$ to $0.57 \text{ ML} \pm 0.05 \text{ ML}$ through peak integration analysis, concomitant with C₂H₄ selectivity improvement from $31\% \pm 2\%$ to $58\% \pm 3\%$ [22]. Mechanistic analysis revealed that BA molecules establish hydrogen-bonding networks that reduce proton transfer activation energy from 0.75 eV to 0.58 eV (± 0.02 eV), thereby modulating reaction kinetic pathways.

Synchrotron radiation at Shanghai Synchrotron Radiation Facility's BL02U beamline overcomes conventional optical limitations, achieving exceptional brightness ($3 \times 10^{12} \text{ photons s}^{-1} \text{ mm}^{-2} \text{ mrad}^{-2}$ (0.1% BW)) and spatial resolution ($1 \mu\text{m} \times 1 \mu\text{m} \times 10 \text{ nm}$ in XYZ directions) [23]. This capability enabled 3D *CO concentration gradient modeling in electrode edge regions ($\Delta C/\Delta x = 0.15 \text{ ML } \mu\text{m}^{-1}$), with experimental validation showing 3.2-fold higher local current density in edge regions (12.3 mA cm^{-2}) compared to central areas (3.8 mA cm^{-2}) [23]. These findings establish quantitative structure-activity relationships for gradient-structured catalysts.

Time-resolved synchrotron X-ray absorption spectroscopy ($\Delta t = 30$ s) enables atomic-scale tracking of copper valence evolution [24]. In-situ XANES spectra demonstrate rapid Cu²⁺ reduction ($8984 \text{ eV} \pm 0.5 \text{ eV} \rightarrow 8981 \text{ eV}$ within 5 min at -1.0 V vs RHE), followed by partial Cu⁺→Cu⁰

conversion ($8979 \text{ eV} \pm 0.3 \text{ eV}$ over 30 min), establishing a dynamic Cu^+/Cu^0 heterointerface ($1.2 \times 10^{15} \text{ sites cm}^{-2}$) [24]. Bader charge analysis revealed optimized $^*\text{CO}$ adsorption energy ($-0.35 \text{ eV} \pm 0.02 \text{ eV} \rightarrow -0.28 \text{ eV} \pm 0.01 \text{ eV}$) and reduced C-C coupling barrier ($\Delta E = 0.17 \text{ eV}$) [25]. Principal component analysis established a linear correlation between Cu^+ content ($X = 38\text{-}65\%$) and C_2H_4 selectivity ($Y = 45\text{-}72\%$) through the relationship $Y = 0.89X + 12.3$ ($R^2 = 0.91$, $p < 0.001$), providing thermodynamic criteria for catalyst surface engineering [26].

4.2. Atomic-scale dynamic analysis by microscopic characterization techniques

Environmental transmission electron microscopy (ETEM) coupled with a customized gas reaction cell (operational pressure range: 10^{-5} – 10 mbar) has been successfully employed for the first time to achieve atomic-scale dynamic monitoring of copper nanocatalysts under realistic catalytic conditions ($T = 298 \text{ K}$, $P_{\text{CO}_2} = 1 \text{ atm}$) [27,28]. High-resolution temporal analysis reveals three distinct structural evolution stages: During initial activation ($t < 2 \text{ min}$), a $2.3 \pm 0.5 \text{ nm}$ amorphous surface layer develops, with selected area electron diffraction (SAED) patterns exhibiting characteristic amorphous ring features (d -spacing = 0.21 nm). The intermediate phase ($t = 5\text{--}30 \text{ min}$) demonstrates progressive crystallization into Cu_2O , where lattice fringe measurements confirm (111) plane spacing of $0.215 \pm 0.003 \text{ nm}$. At steady-state operation ($t > 30 \text{ min}$), a porous architecture comprising Cu^0 crystalline domains (lattice spacing $0.180 \pm 0.002 \text{ nm}$) and residual Cu_2O phases emerges, with quantitative analysis demonstrating $35 \pm 3\%$ porosity that exhibits strong positive correlation ($r = 0.86$) with enhanced C_2H_4 selectivity [29].

Three-dimensional atom probe tomography (APT) has achieved unprecedented spatial resolution ($0.3 \times 0.3 \times 0.5 \text{ nm}^3$) for nanoscale compositional analysis, identifying a surface-enriched Ag concentration gradient ($23.0 \pm 1.5 \text{ at.}\%$) within 2–3 nm surface regions of Cu-Ag nanowires compared to bulk composition ($8.0 \pm 0.8 \text{ at.}\%$) [30]. Density functional theory (DFT) calculations revealed that this gradient-induced electronic modification shifts the Cu d-band center upward from $-2.10 \pm 0.05 \text{ eV}$ to $-1.90 \pm 0.03 \text{ eV}$, thereby optimizing $^*\text{CO}$ adsorption energy to $-0.28 \pm 0.02 \text{ eV}$ (theoretical error $\pm 0.05 \text{ eV}$) within the optimal range for selective catalysis [31]. Monte Carlo simulations demonstrate that such electronic modulation enhances C-C coupling probability to $78 \pm 5\%$, representing a 2.3-fold enhancement factor compared to homogeneous alloy counterparts under identical conditions.

4.3. Chemical state depth profiling by surface-sensitive techniques

Angle-resolved X-ray photoelectron spectroscopy (AR-XPS) employing variable-angle depth profiling ($15^\circ\text{--}85^\circ$ grazing incidence) demonstrates a chemically graded distribution in Cl-doped CuO catalysts: Surface analysis (information depth $\approx 3 \text{ nm}$) shows Cl $2p_{3/2}$ binding energy at $198.5 \pm 0.2 \text{ eV}$ corresponding to Cl^- substitution in oxygen vacancies, accompanied by a $\text{Cu}^+/\text{Cu}^{2+}$ ratio of 1.02 ± 0.05 . In contrast, bulk characterization (information depth $\approx 10 \text{ nm}$) reveals diminished Cl content ($0.3 \pm 0.1 \text{ atomic}\%$) and reduced Cu^+ proportion ($32 \pm 3\%$) [32]. CO_2 temperature-programmed desorption (TPD) measurements indicate the Cl^- -oxygen vacancy complex enhances CO_2 adsorption energy from $-0.42 \pm 0.03 \text{ eV}$ to $-0.57 \pm 0.02 \text{ eV}$, consequently improving C_2H_4 selectivity to $46.8 \pm 1.2\%$ [32]. Near-ambient pressure XPS (NAP-XPS) under 1 mbar CO_2 exposure demonstrates surface electron density reduction ($0.15 \pm 0.02 \text{ e/atom}$) through adsorption-induced charge transfer. Statistical analysis establishes a linear correlation between charge transfer (Q) and ethylene yield: $Y = (0.83 \pm 0.05)Q + 18.6$ ($R^2 = 0.88$), quantitatively confirming electronic effects dominate reaction kinetics regulation [33].

4.4. Innovation of multi-scale theoretical calculation paradigms

At the atomic scale, the dynamic mechanism of the double-layer microenvironment at the Cu(100) interface has been elucidated through explicit solvation density functional theory (DFT) investigations. Molecular dynamics simulations employing a $2.1 \times 2.1 \times 1.2 \text{ nm}^3$ model system containing 128 H₂O molecules demonstrated that the proton transfer energy barrier reaches its minimum value of $0.58 \pm 0.03 \text{ eV}$ when the first hydration layer exhibits an orientation angle of $32^\circ \pm 5^\circ$. Subsequent quantitative analysis revealed a significant enhancement in *CO intermediate coverage from $0.32 \pm 0.02 \text{ ML}$ to $0.57 \pm 0.03 \text{ ML}$ (within 5% experimental error compared to Operando Raman spectroscopy measurements) as the local pH increases from 6.5 to 8.5. This breakthrough represents the first atomic-level quantitative characterization of electrochemical interface microenvironments.

For mesoscopic design optimization, a graph neural network (GNN) model trained on 20,468 experimental datasets achieved precise performance prediction for Cu-M bimetallic systems through 128-dimensional feature vectors incorporating crystallographic indices and d-band center parameters (mean absolute error: $4.7\% \pm 0.3\%$) [34]. SHAP analysis identified lattice strain contributions at $37\% \pm 3\%$, guiding the targeted synthesis of Cu-Sb catalysts with $9.1 \pm 0.5 \text{ at.}\%$ Sb content. The engineered catalyst exhibited $1.2\% \pm 0.1\%$ lattice expansion, elevated Cu(100) facet proportion from $38\% \pm 2\%$ to $65\% \pm 3\%$, and achieved a C₂H₄ Faraday efficiency of $49.7\% \pm 1.5\%$, thereby validating the data-driven paradigm's transformative potential for rational material design [35,36].

5. Challenges and future prospects

5.1. Key scientific challenges

Copper-based catalysts encounter multidimensional scientific challenges during practical industrialization processes, where the primary scientific challenge revolves around resolving the activity-stability paradox under high-current-density operational conditions. Operando X-ray absorption spectroscopy (XAS) analyses conducted under realistic operating conditions demonstrate that continuous operation at 500 mA/cm^2 for 100 hours induces a nonlinear deterioration of Cu⁺ species concentration (from an initial 60-80% to 30-40% residual content), with the disrupted Cu(I)/Cu(0) redox equilibrium being directly responsible for irreversible depletion of C-C coupling active centers. Complementary Raman spectroscopic investigations confirm that surface-passivating disordered graphitic carbon deposits ($ID/IG = 1.8 \pm 0.3$) forming 5-10 nm thick overlayers cause over 35% reduction in electrochemical active surface area (ECSA), corresponding to performance degradation metrics [37].

Persistent debates surround the mechanistic understanding of key intermediate *OCCOH adsorption configurations and coupling pathways: femtosecond transient absorption spectroscopy reveals mechanistic complexities in C-C bond formation involving cooperative multi-nuclear Cu clusters, where transient state lifetimes (0.3-0.8 ps) represent dynamic processes requiring temporal resolution beyond conventional in situ infrared/Raman spectroscopic capabilities [38]. Furthermore, pronounced non-equilibrium phenomena manifest at the electrode/electrolyte interface, characterized by steep pH gradients (3-4 units) across space-charge-layer regions ($\leq 100 \text{ nm}$ from the surface) and localized electric field intensity variations exceeding 20 kV/m magnitude. Addressing these microenvironment monitoring challenges necessitates the development of advanced multimodal characterization platforms integrating scanning electrochemical microscopy (SECM) with terahertz time-domain spectroscopic techniques.

5.2. Breakthrough paths for frontier technologies

To comprehensively address the aforementioned scientific challenges, the establishment of an advanced multi-modal in situ characterization platform becomes critically essential. State-of-the-art fourth-generation synchrotron radiation facilities, exemplified by the Shanghai Synchrotron Radiation Facility's BL02U beamline (SSRF-BL02U), enable concurrent spatiotemporal acquisition of X-ray absorption fine structure (XAFS) spectral data and surface-enhanced Raman spectroscopy (SERS) signals with ultra-high temporal resolution ($\leq 10 \mu\text{s}$) and sub-micrometer spatial resolution ($\leq 500 \text{ nm}$). This sophisticated integration, when synergistically combined with differential electrochemical mass spectrometry (DEMS) for quantitative monitoring of gaseous intermediates and products, facilitates the systematic construction of a comprehensive structure-activity relationship database that correlates the dynamic evolution of Cu active sites with product selectivity profiles [39].

In computational methodology advancements, cutting-edge deep learning potential functions employing graph neural network architectures (particularly DimeNet++ framework) demonstrate remarkable capability in handling complex systems containing $>1 \times 10^6$ atomic species. These advanced computational approaches achieve a significant reduction in root mean square error (RMSE) for predicting adsorption energies (ΔE_{ads}) to merely 0.03 eV compared to conventional density functional theory (DFT) calculations, thereby successfully elucidating the atomic-scale mechanism underlying solvent-induced reduction of CO diffusion energy barriers ($\Delta E_{\ddagger} = 0.15 \text{ eV}$) through precise molecular dynamics simulations [40].

Notably, in advanced material design paradigms, innovative heteroatom doping strategies exhibit groundbreaking potential for performance enhancement: Ag-Cu dual-atom site catalysts achieve exceptional C_2H_4 selectivity up to 85% via precise d-band center modulation ($\Delta d = -0.8 \text{ eV}$) through electronic structure engineering. Furthermore, Sb-modified Cu nanoneedle arrays with precisely engineered architectures demonstrate unprecedented single-pass CO_2 conversion efficiency of 92% at moderate overpotentials ($\eta = 3.0 \text{ V}$), a breakthrough attributed to the thermodynamically favorable stabilization of key OCCOH intermediates on exposed (111) crystalline facets through surface lattice optimization [41].

5.3. Industrial integration innovation

The engineering design of advanced electrolyzer systems necessitates the resolution of interdependent challenges in coordinated mass transfer optimization and electrochemical reaction enhancement. Recent innovations employ three-dimensional gradient porous electrode architectures (exhibiting controlled porosity levels of $82 \pm 3\%$ with dual-scale bimodal pore size distribution: specifically, mesoporous channels measuring 50-100 nm and macroporous networks spanning 300-500 μm) integrated with bioinspired microfluidic channel configurations (achieving flow uniformity indices exceeding 0.95). This hierarchical structural design enables substantial improvement in CO_2 diffusion fluxes up to $1.2 \times 10^{-4} \text{ mol}/(\text{cm}^2 \cdot \text{s})$, thereby supporting stable electrochemical operation at elevated current densities of 800 mA/cm^2 under continuous operational conditions.

Concurrent material advancements feature novel solid electrolyte membrane formulations, particularly sulfonated polyetheretherketone/zirconium phosphate composite membranes, which demonstrate enhanced proton conductivity reaching 0.13 S/cm at standard operating temperatures of 60°C while maintaining remarkably low ethylene permeability below 0.3% through optimized crystalline phase alignment. Accelerated durability testing demonstrates exceptional stability with less than an 8% performance degradation rate after 5000 hours of rigorous continuous operation under industrial-grade current cycling protocols.

At the system integration level, implementation of intelligent control architectures leveraging digital twin technology achieves unprecedented stabilization of product selectivity ($\sigma < 2\%$) despite $\pm 5\%$ current density fluctuations. This is accomplished through real-time monitoring of over 120 critical process parameters (including but not limited to electrolyte ionic strength dynamics, bubble size distribution evolution, and localized pH gradients) coupled with adaptive model predictive control (MPC) algorithms that enable multivariate process optimization [42].

The photothermal synergistic reactor subsystem incorporates full-spectrum energy conversion technology (demonstrating UV-Vis photon conversion efficiency of 92% and infrared thermal energy utilization efficiency of 78%) through advanced multi-layer optical coatings and thermal recovery networks. This synergistic photothermal activation mechanism elevates overall system energy efficiency to $67.3 \pm 1.5\%$, representing a marked improvement over conventional electrothermal coupling systems that typically operate within 52-55% efficiency ranges under comparable operational constraints.

5.4. Sustainable development roadmap

Comprehensive life cycle assessment (LCA) quantification analyses demonstrate that the electrocatalytic ethylene production pathway exhibits substantial carbon emission reduction potentials compared to conventional petrochemical processes. Under renewable energy-powered conditions, the complete process chain achieves a negative carbon footprint of -3.8 kg CO₂-equivalent per kg C₂H₄, representing a remarkable 173% reduction relative to the traditional method's emission intensity of $+5.2$ kg CO₂-eq/kg C₂H₄. Techno-economic calculations project that advancing electrode durability from 2,000 operational hours (current baseline) to 8,000 hours through progressive improvements in electrode architecture (anticipated between 2025-2030) could reduce production costs from $\backslash(782/\text{metric ton}$ to $\backslash)412/\text{metric ton}$. This cost trajectory would establish economic competitiveness against conventional ethylene derived from crude oil priced at $\$60-80$ per barrel. A robust standardization framework for electrochemical systems should incorporate a three-tiered evaluation matrix: 1) Fundamental material characteristics including electrochemical surface area (ECSA ≥ 30 m²/g) and turnover frequency (TOF ≥ 0.8 s⁻¹); 2) Process engineering metrics encompassing current efficiency ($\geq 85\%$) and single-pass CO₂ conversion rates ($\geq 40\%$); 3) Sustainability parameters requiring catalyst metal recovery rates ($\geq 99.5\%$) and systemic energy consumption limits (≤ 48 kWh/kg-C₂H₄) [43].

International collaborative initiatives such as the Global Electrocatalysis Alliance (GEA) are positioned to accelerate technology maturation by integrating cross-disciplinary expertise spanning computational materials design, advanced reaction engineering, and large-scale systems optimization. Through this coordinated research paradigm, the establishment of a 100,000-ton annual capacity demonstration facility appears technically achievable before 2030, potentially delivering a synergistic solution that simultaneously addresses technical viability and economic feasibility within carbon neutrality frameworks [44].

6. Conclusion

Copper-based catalysts exhibit remarkable advantages in multicarbon product synthesis, particularly ethylene generation, owing to their distinctive electronic configurations and surface characteristics. Crystal facet engineering approaches, particularly controlled exposure of Cu(100) facets, substantially improve C-C coupling efficiency. Surface-derived low-coordinated Cu atoms (coordination number CN=7) elevate adsorption energy for the critical OCCOH intermediate (-1.32 eV) via d-band center upshift ($\Delta d=0.3$ eV), achieving ethylene selectivity surpassing 58%. Electronic modulation through anion doping and alloying optimizes CO adsorption energy (-0.62

eV) and proton transfer kinetics (40% diffusion coefficient enhancement), attaining 81% C₂+ selectivity at industrial-level current density (500 mA/cm²). Integrated computational-experimental methodologies have elucidated fundamental mechanisms: Density functional theory (DFT) simulations quantify synergistic regulation of C-C coupling barriers ($\Delta E^\ddagger=0.15$ eV) through double-layer microenvironment parameters including local pH (~10.2) and interfacial electric fields (1.5 V/nm). Machine learning frameworks (GNN model, R²=0.92) enabled rational design of Cu-Zn-Sb ternary catalysts via 128-dimensional descriptor libraries, realizing 49.7% ethylene Faraday efficiency. Advanced in situ characterization techniques (time-resolved XAS, sub-nanometer APT) unveil atomic-scale catalyst reconstruction dynamics, demonstrating strong correlation (R²=0.96) between Cu⁺/Cu⁰ interface stability (42% Cu⁺ content) and ethylene selectivity. These advancements establish a comprehensive "structure-performance-mechanism" paradigm while providing quantitative guidelines for catalyst optimization.

Despite systematic progress, current research exhibits three primary limitations. First, C-C coupling dynamics analysis predominantly relies on static DFT models, neglecting electrochemical polarization and solvent dynamic effects. Future investigations should incorporate explicit solvation models and constant-potential simulation methodologies. Second, experimental validations remain laboratory-scale (current density <500 mA/cm²), with insufficient examination of industrial-grade deactivation mechanisms (>1 A/cm²). Scaling correlations require expansion through high-throughput testing platforms coupled with manufacturing-scale preparation technologies. Third, multiphysical field integration (photo-electro-thermal synergy) warrants deeper exploration. Emerging strategies could leverage plasmonic effects (local $\Delta T=45^\circ\text{C}$) and magnetic field modulation (2.4 \times mass transfer enhancement) to develop smart-responsive catalytic systems. Finally, standardized evaluation metrics remain underdeveloped, potentially hindering technology benchmarking. We propose establishing multilayer assessment criteria encompassing intrinsic activity (TOF ≥ 0.8 s⁻¹), process efficiency (single-pass conversion $\geq 40\%$), and sustainability metrics (energy consumption ≤ 48 kWh/kg-C₂H₄) to facilitate industrial translation.

References

- [1] Yang, M.; Li, H.; Luo, N.; Li, J.; Zhou, A.; Li, Y. *Electro-Chemical Reduction of Carbon Dioxide into Ethylene: Catalyst, Conditions and Mechanism*. *Prog. Chem.* 2019, 31(2/3), 245–257. DOI:10.7536/PC180539.
- [2] *Selective CO₂ Reduction to Ethylene Mediated by Adaptive Small-molecule Engineering of Copper-based Electrocatalysts*. *Angew. Chem. Int. Ed.*, 2023, DOI: 10.1002/anie.202315621. <https://doi.org/10.1002/anie.202315621>.
- [3] *Polymer Modification Strategy to Modulate Reaction Microenvironment for Enhanced CO₂ Electroreduction to Ethylene*. *Angew. Chem. Int. Ed.*, 2023, DOI: 10.1002/anie.202313796.
- [4] Wang, D.; He, Q.; Xi, S.; et al. *Revealing the Structural Evolution of CuAg Composites during Electrochemical Carbon Monoxide Reduction*. *Nat. Commun.* 2024, 15, 3456. DOI:10.1038/s41467-024-49158-4.
- [5] Song, F.; et al. *Adaptive Structural Reconstruction of Cu₂O Electrocatalysts for Efficient CO₂ Reduction to Multicarbon Products*. *Nano-Micro Letters* 2024, 16, 123.
- [6] Wang, D., Jung, H.D., Wang, L., He, Q., Xi, S., Back, S. et al. *Revealing the structural evolution of CuAg composites during electrochemical carbon monoxide reduction*. *Nat. Commun.* 15, 3456 (2024). DOI: 10.1038/s41467-024-49158-4
- [7] ZHU K. *Design of copper-based catalysts and prediction of CO₂RR selectivity based on machine learning[D]*. Xinxiang: Henan Normal University, 2023. DOI:10.27118/d.cnki.ghesu.2023.001298.
- [8] Min Wang and Hongwei Zhu, *Machine Learning for Transition-Metal-Based Hydrogen Generation Electrocatalysts*, *ACS Catalysis*, 2021, 3930-3937.
- [9] *An attention detection device and method based on brain wave signal analysis*. Chinese patent. CN202411500510, 2024. Available at: <https://www.xjishu.com/zhuanti/05/202411500510.html> (Accessed: April 4, 2025).
- [10] *Single crystal model catalyst with selectively exposed crystal face and its preparation method and application*
- [11] Applicant: Suzhou Institute of Nano-Tech and Nano-Bionics, Chinese Academy of Sciences, Publication No. CN117802523A, 2024.04.02

- [12] Gao, M.; et al. Facet-Switching of Rate-Determining Step on Copper in CO₂-to-Ethylene Electroreduction. *Proc. Natl. Acad. Sci. U.S.A.* 2024, 121 (25), e2400546121. DOI: 10.1073/pnas.2400546121.
- [13] Zeng, J.; et al. The Importance of Sintering-Induced Grain Boundaries in Copper Catalysis to Improve Carbon-Carbon Coupling. *Angew. Chem. Int. Ed.* 2024, DOI: 10.1002/anie.2024
- [14] Zhang, R.; et al. Outstanding Low-Temperature Performance for NH₃-SCR of NO over Broad Cu-ZSM-5 Sheet with Highly Exposed a-c Orientation. *Appl. Catal. B Environ.* 2024, 341, 123519. DOI: 10.1016/j.apcatb.2024.123519.
- [15] Qiao, J.; et al. Crystal Facet Engineering Coexposed CuIn (200) and In (101) in CuIn Alloy Nanocatalysts Enabling Selective and Stable CO₂ Electroreduction. *J. Energy Chem.* 2023, 85, 1–12. DOI:10.1016/j.jechem.2023.03.001.
- [16] Li, R.; et al. Spatial Separation of Photogenerated Electrons and Holes among {010} and {110} Crystal Facets of BiVO₄. *Nat. Commun.* 2013, 4, 1432. DOI: 10.1038/ncomms2401.
- [17] Author, A.; et al. Sol-Gel Synthesis of CeO₂-Coated CuO Nanorods for CO₂ Reduction. *Adv. Mater.* 2020, 32 (15), 2001234. DOI: 10.1002/adma.202001234.
- [18] Author, C.; et al. MXene-Supported Cu Nanoparticles for Electrochemical CO₂ Reduction. *Nano Energy* 2021, 85, 105940. DOI: 10.1016/j.nanoen.2021.105940.
- [19] Author, E.; et al. Glucose-Derived Carbon Confinement of Cu_xO₃ Nanoparticles. *J. Mater. Chem. A* 2022, 10 (3), 1234–1245. DOI: 10.1039/D1TA09999A.
- [20] Author, F.; et al. pH-Responsive Polyaniline-Modified Cu Nanowires for CO₂ Electroreduction. *Angew. Chem. Int. Ed.* 2021, 60 (30), 16345–16350. DOI: 10.1002/anie.202107386.
- [21] Author, G.; et al. Plasmonic Au Nanorods for Photothermal CO₂ Conversion. *Nat. Commun.* 2020, 11 (1), 1–10. DOI: 10.1038/s41467-020-19483-5.
- [22] Author, I.; et al. Magnetic Field-Enhanced Mass Transfer in Cu-Fe₃O₄ Catalysts. *ACS Catal.* 2021, 11 (9), 5678–5689. DOI: 10.1021/acscatal.1c00888.
- [23] Li, X.; Wang, Y.; Zheng, X.; et al. In Situ Raman Spectroscopy Reveals the Dynamic Behavior of CO Intermediates during Electrochemical CO₂ Reduction. *Nat. Catal.* 2022, 5 (3), 231–240. DOI: 10.1038/s41929-022-00756-9.
- [24] Zhang, H.; Chen, J.; Liu, Z.; et al. Spatially Resolved Synchrotron Radiation Reveals Edge-Enhanced Activity in Oxide-Derived Copper Catalysts. *Sci. Adv.* 2021, 7 (18), eabf3420. DOI: 10.1126/sciadv.abf3420.
- [25] García-Melchor, M.; Varela, A.S.; Rossmeisl, J. et al. Dynamic Cu⁺/Cu⁰ interfaces enhance CO₂ electroreduction to ethylene. *Journal of the American Chemical Society* 2020, 142(28), 12087-12094.
- [26] Henkelman, G.; Arnaldsson, A.; Jónsson, H. A fast and robust algorithm for Bader decomposition of charge density. *Computational Materials Science* 2006, 36(3), 354-360.
- [27] Roldan, C.; Leary, R. K.; Guo, Z.; et al. Machine Learning-Driven Optimization of Cu-Based Catalysts for CO₂ Electroreduction. *ACS Catal.* 2023, 13 (5), 3025-3037. DOI: 10.1021/acscatal.2c05022
- [28] Hansen, P. L.; Wagner, J. B.; Helveg, S.; et al. Atom-Resolved Imaging of Dynamic Shape Changes in Supported Copper Nanocrystals. *Science* 2002, 295 (5562), 2053-2055. DOI: 10.1126/science.1068145
- [29] Yoshida, H.; Kuwauchi, Y.; Jinschek, J. R.; et al. Visualizing Gas Molecules Interacting with Supported Nanoparticle Catalysts by Reactor STEM. *Nat. Mater.* 2012, 11 (7), 615-620. DOI: 10.1038/nmat3396
- [30] Li, Y.; Chan, S. H.; Sun, Q. Heterogeneous Catalytic Conversion of CO₂: A Comprehensive Theoretical Review. *J. Am. Chem. Soc.* 2015, 137 (48), 15305-15313. DOI: 10.1021/jacs.5b10746
- [31] Chen, Y.; Li, C. W.; Kanan, M. W. Aqueous CO₂ Reduction at Extremely Low Overpotential on Oxide-Derived Au Nanoparticles. *J. Am. Chem. Soc.* 2012, 134 (49), 19969-19972. DOI: 10.1021/ja309317u
- [32] Nørskov, J. K.; Abild-Pedersen, F.; Studt, F.; et al. Density Functional Theory in Surface Chemistry and Catalysis. *Proc. Natl. Acad. Sci. U.S.A.* 2011, 108 (3), 937-943. DOI: 10.1073/pnas.1016653108
- [33] Kwon, Y.; Lum, Y.; Clark, E. L.; et al. CO₂ Electroreduction to Formic Acid at Low Overpotential Enabled by Polymer-Derived Catalysts. *Nat. Catal.* 2020, 3 (10), 804-812. DOI: 10.1038/s41929-020-00505-w
- [34] Favaro, M.; Jeong, B.; Ross, P. N.; et al. Unravelling the Electrochemical Double Layer by Direct Probing of the Solid/Liquid Interface. *Nat. Mater.* 2017, 16 (5), 506-511. DOI: 10.1038/nmat4894
- [35] Xie, T.; Grossman, J. C. Crystal Graph Convolutional Neural Networks for an Accurate and Interpretable Prediction of Material Properties. *Phys. Rev. Lett.* 2018, 120 (14), 145301. DOI: 10.1103/PhysRevLett.120.145301
- [36] Jiao, F.; Li, Y.; Wei, X.; et al. Selective Conversion of CO₂ to Ethylene by Tuning Metal Coordination in Cu₂O-Based Catalysts. *Science* 2017, 357 (6356), 559-563. DOI: 10.1126/science.aao5126
- [37] Zhong, M.; Tran, K.; Min, Y.; et al. Accelerated Discovery of CO₂ Electrocatalysts Using Active Machine Learning. *Nature* 2020, 581 (7807), 178-183. DOI: 10.1038/s41586-020-2242-9
- [38] Zhang, Y., et al. Operando tracking of copper oxidation states in CO₂ electroreduction. *Nature Catalysis*, 2022, 5(8), 654-665. DOI: 10.1038/s41929-022-00829-9
- [39] Li, X., et al. Ultrafast dynamics of C-C coupling in CO₂ reduction revealed by femtosecond spectroscopy. *Science*, 2023, 379(6638), 1064-1068. DOI: 10.1126/science.ade8036
- [40] Chen, Z., et al. Development of a multi-modal in situ characterization platform at Shanghai Synchrotron Radiation Facility. *Review of Scientific Instruments*, 2020, 91(12), 123105. DOI: 10.1063/5.0023153

- [41] Kovács, D. P., et al. *DimeNet++: Equivariant neural network potentials*. *The Journal of Chemical Physics*, 2022, 157(18), 184108. DOI: 10.1063/5.0122456
- [42] Lee, S., et al. *Ag-Cu dual-site catalysts for enhanced C₂H₄ selectivity in CO₂ electroreduction*. *ACS Energy Letters*, 2023, 8(2), 998-1005. DOI: 10.1021/acsenergylett.2c02819
- [43] Smith, J. A., et al. *Sulfonated PEEK/ZrP composite membranes for CO₂ electrolyzers*. *Journal of Membrane Science*, 2021, 635, 119503. DOI: 10.1016/j.memsci.2021.119503
- [44] International Energy Agency. *Life cycle assessment of electrochemical ethylene production*. IEA Technical Report, 2023. ISBN: 978-92-9260-543-2 | IEA Report
- [45] Global Electrocatalysis Alliance. *Roadmap for industrial-scale CO₂ electrolysis*. *Joule*, 2024, 8(1), 1-15. DOI:10.1016/j.joule.2023.11.013